ARTICLE

CO Oxidation by BN−Fullerene Cage: Effect of Impurity on the Chemical Reactivity

Sandeep Nigam and Chiranjib Majumder*

Chemistry Division, Bhabha Atomic Research Center, Trombay, Mumbai-85, India

ABSTRACT Using state of the art spin-polarized density functional theory it is found that a chemically inert $(BN)_{36}$ cluster can be activated by incorporating magnetic nanoparticles inside it. To illustrate this aspect we have calculated the geometries and electronic structure of $Fe(BN)_{36}$ and $Fe_4(BN)_{36}$ clusters, which showed the appearance of gap states localized on the impurity atoms. The reaction of O_2 molecules with these clusters results in weak interaction and an elongation of the O−O bond. Further interaction of this complex species with an incoming CO molecule leads to the formation of CO_2. The reaction mechanism has been investigated *via* Langmuir−Hinshelwood and Elay−Rideal routes, and the minimum energy path calculations are performed using the elastic band method. These results have implications in designing novel materials based on metal nanoparticles for potential applications as industrial catalyst.

KEYWORDS: nanomaterials · BN–fullerene · DFT · catalysis · metal clusters

A unique aspect of nanotechnology is the vastly increased ratio of surface area to volume in many materials which opens new possibilities in surface-based science, such as catalysis.[1–5] Thus, research in nanotechnology and nanoscience is expected to have a great impact on the development of new catalysts. A detailed understanding of the chemistry of nanostructures and the ability to control materials on the nanometer scale will ensure a rational and cost-efficient development of new and more capable catalysts for chemical industry. In recent times, nanocatalysis has emerged as one of the most exciting subfields of nanoscience.[6–16] A large amount of experimental and theoretical work showed the catalytic behavior of gold clusters, which are in fact noble metals in the bulk. Therefore, at a smaller size the electronic properties of the materials could be widely different from their bulk properties. Small transition metal clusters have been projected as the potential candidates for their applications in catalysis. However, free metallic particles are susceptible to undergo chemical reactions easily, which changes their physicochemical characteristics and, therefore, deters them from practical applications. To overcome this bottleneck, these active particles can be encapsulated inside an inert material. In fact, boron nitride is well-known coating material to prevent iron from its oxidation. It has been envisaged that if the thickness of the coating of boron nitride is reduced then we may expect to see a moderate level of reactivity of these materials. An empty cage nanocluster, which is chemically inert with a large energy gap, will be an ideal choice to design such material.

Like carbon nanomaterials, boron nitride (BN) forms empty cage nanostructures in different shapes like fullerenes, nanotubes, nanohorns, *etc.*[17–33] Although the BN pair is isoelectronic with a pair of carbon atoms, their bulk electronic properties differ considerably. While C-based nanomaterials show metallic or semiconducting properties, BN-based nanostructures form wide gap insulators. In fact, boron nitride systems are more stable than carbon materials in terms of thermal and chemical stability. On the basis of these criteria, it is proposed that a BN nanostructure can be functionalized to tune its physio-chemical properties for its potential applications.[30–32] Oku and co-workers have produced a series of cage-like BN clusters of different sizes.[17–28] After this, a large amount of experimental and theoretical studies have been performed to understand the geometry and energetic of the $(BN)_{36}$ cage cluster.[33–38] These studies have revealed that $(BN)_{36}$ cluster forms an isolated single-shelled BN fullerene with overall dimensions of 8−9 Å and proposed octahedron geometry for this BN cluster.

The presence of impurity metal atoms or clusters inside the nanocage or nanotubes during their synthesis can signifi-

*Address correspondence to chimaju@barc.gov.in.

Received for review March 9, 2008 and accepted June 02, 2008.

Published online June 11, 2008.
10.1021/nn8001455 CCC: $40.75

cantly modify the physicochemical properties. To understand this effect, many experimental and theoretical studies have been reported on the metal-encapsulated BN nanomaterial.[39–45] In fact it is found that the transition metals like Fe, Co, and Ni are the most effective catalysts for the formation of BN nanotubes.[43] Oku and co-workers produced Fe-filled BN nanotubes and investigated them by high-resolution electron microscopy and energy dispersive X-ray spectroscopy.[46] Recently, boron nitride nanocapsules encaging Fe and Co nanoparticles have been synthesized, and their magnetic properties were investigated.[29]

The CO oxidation reaction is of practical importance for the control of the environmental pollution that results from combustion processes. Late transition metal surfaces have been the most widely studied example for this purpose.[47,48] While noble metals (Pd, Pt) are costly, transition metals like Fe, Co, and Ni are known for their propensity to oxidation. Now to design a material for catalysis the basic requirement is that the host matrix should interact with the reactant molecules weakly. On the basis of these considerations it was envisaged that the opposite chemical behavior of transition metal and BN clusters can be used to design a novel composite material which will show catalytic behavior. Indeed, in our work we find that even a small doping of Fe inside the large gap $(BN)_{36}$ cluster is able to activate the cage. Consequently, the adsorption of O_2 on the $Fe(BN)_{36}$ cluster leads to stretching of the O−O bond comparable to the peroxo and superoxo[49] state, which facilitates the oxidation of CO molecule.

RESULTS AND DISCUSSION

To start with, the accuracy of the computational method applied in this work was tested by computing the structure and binding energy of O_2, CO, and CO_2 molecules. The results (Table S1 in the Supporting Information) showed good agreement between calculated and experimental values. For the $(BN)_{36}$ cluster, the ground-state geometry shows a hollow cage with 32 hexagonal rings and six squares oriented in an octahedral arrangement (O_h symmetry). The average binding energy of the $(BN)_{36}$ cluster has been estimated to be 6.76 eV/atom. The higher stability of the BN cage is further substantiated by its large energy gap of 4.95 eV. These results are found to be in excellent agreement with previously published works.[56–61] To obtain the lowest energy atomic configurations of the Fe_4 cluster, apart from several initial structures, three important starting configurations *viz.* planar rhombus, bent rhombus, and tetrahedron with variations in the spin states were considered. The lowest energy structure of the Fe_4 cluster showed distorted tetrahedron with an average magnetic moment of 3.5 μ_B/atom (total spin moment = 14 μ_B). The next higher energy isomer, with similar atomic structure but lower spin state (total spin moment = 12 μ_B), is found to be 0.14 eV higher in energy. These results are in excellent agreement with previously reported ones.[62]

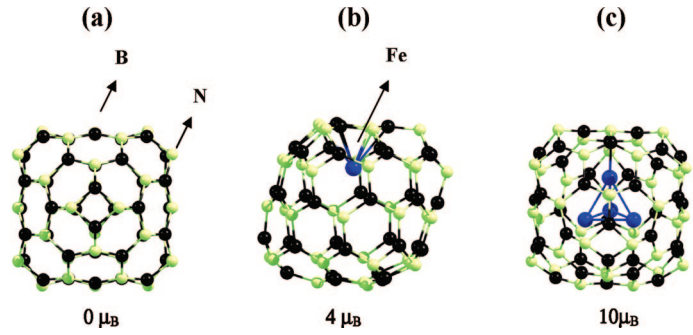

Figure 1. Lowest lying isomer of (a) $(BN)_{36}$, (b) $Fe(BN)_{36}$, and (C) $Fe_4(BN)_{36}$ clusters.

For the $Fe(BN)_{36}$ cluster, the equilibrium geometry (shown in Figure 1) was obtained by optimizing four initial guess structures; (i) the Fe atom occupying the center position of the cage, (ii) the Fe atom is placed off center and close to the tetragonal ring, (iii) the Fe atom is placed off center and close to the hexagonal ring, and (iv) the Fe atom is connected to the bridge site of the tetragonal and hexagonal ring. The lowest energy structure shows that the Fe atom favors a connection at the hexagonal ring from inside. The total spin moment of this isomer was found to be 4 μ_B. From the geometrical point of view, the presence of Fe inside the $(BN)_{36}$ cage has a very negligible effect on the cage structure. For the $Fe_4(BN)_{36}$ cluster, we have optimized the geometry by placing the Fe_4 inside the cage using all configurations of Fe_4 that have been considered in its free state. This way we have also verified any change in the geometry of the Fe_4 cluster occurring because of the restraints imposed by the confined environment of the cage. The results show that the geometry of the Fe_4 cluster becomes more compact inside the cage and the total spin moment reduces from 14 to 10 μ_B. Moreover, we note that the stability of the Fe_4 cluster inside the cage is enhanced by 0.42 eV in comparison to its free state.

To understand the nature of chemical interaction in these systems we have analyzed the electronic density of states (EDOS) by broadening the electronic energy levels with a Gaussian function (shown in Figure 2). It is found that the incorporation of Fe clusters inside the $(BN)_{36}$ cage introduces energy states in the large gap between highest occupied and lowest unoccupied energy levels of the $(BN)_{36}$ cage. We have also verified the frontier orbitals of the $Fe(BN)_{36}$ and $Fe_4(BN)_{36}$ clusters (shown in Supporting Information, Figure S1), which further corroborates the analysis from the EDOS spectrum. It should be mentioned that despite coating the Fe magnetic clusters by the BN nanocage, the open shell nature of the electronic spectrum shows their intrinsic magnetic nature. The appearance of these gap states in the presence of the Fe clusters results in low-

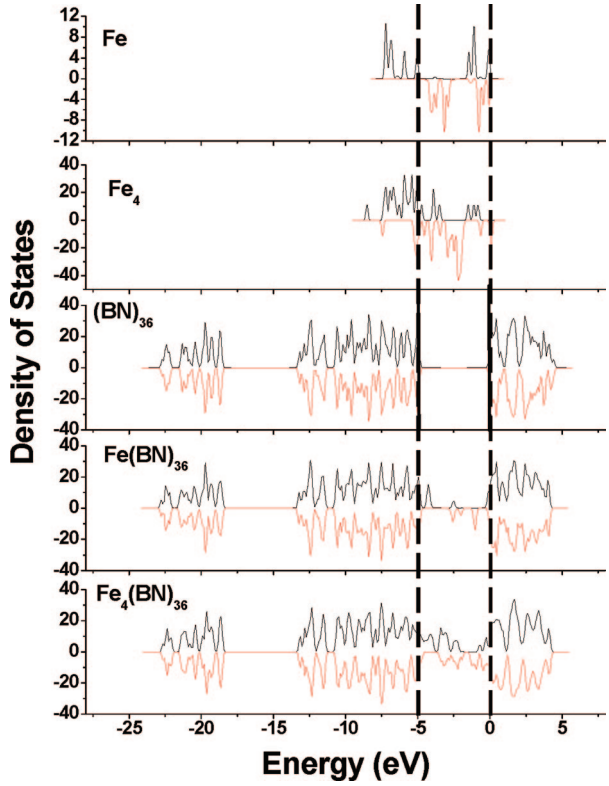

Figure 2. The electronic density of state (EDOS) spectrum of Fe, Fe_4, $(BN)_{36}$, $Fe(BN)_{36}$, and $Fe_4(BN)_{36}$ clusters. The vertical line represents the HOMO and LUMO energy level of the $(BN)_{36}$ cluster.

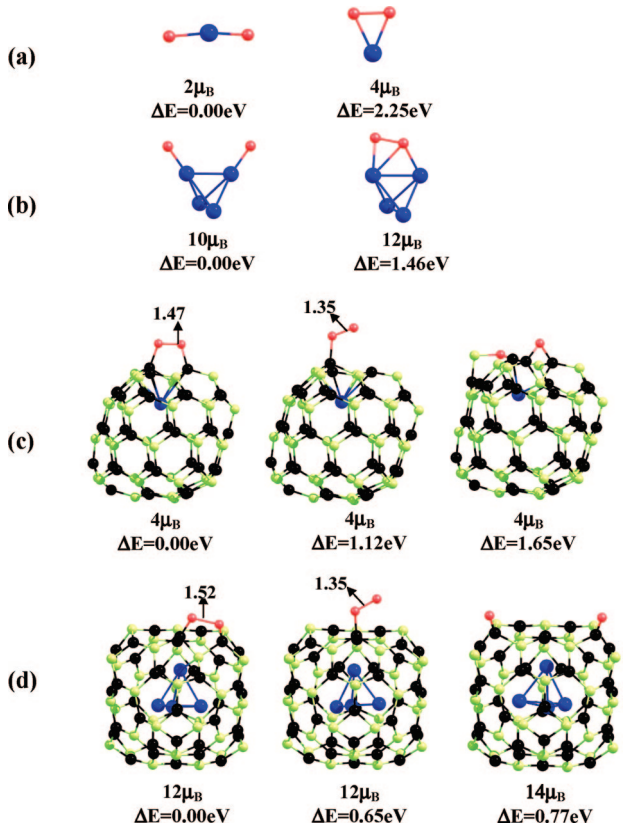

Figure 3. Low lying isomer of (a) FeO_2, (b) Fe_4O_2, (c) $Fe(BN)_{36}O_2$, and (d) $Fe_4(BN)_{36}O_2$ clusters. The relevant spin moments (μ_B) are mentioned along with the structure. Presented bond distances are given in angstroms.

ering the HOMO−LUMO gap of these clusters. This implies an induce reactivity of the BN nanocage by the encapsulation of Fe metal clusters.

Here we discuss the interaction of the O_2 molecule with Fe, Fe_4, $(BN)_{36}$, $Fe(BN)_{36}$ and $Fe_4(BN)_{36}$ clusters. The relevant low-lying isomers with corresponding spin moments are depicted in Figure 3. To start with, we have calculated the interaction of the O_2 molecule with the Fe atom. The lowest energy configuration shows that the interaction of O_2 with Fe leads to the dissociation of the O−O bond and forms an O−Fe−O complex with an interatomic distance of Fe−O = 1.60 Å and an O−Fe−O bond angle of 170° as shown in Figure 3a. The total spin moment of this complex is estimated to be 2 μ_B. The energy released for this reaction $[E(FeO_2) - E(Fe) - E(O_2)]$ is calculated to be 4.32 eV. The other isomer, where the O−O bond does not break but elongates up to 1.48 Å, is significantly higher (ΔE = 2.25 eV) in energy. For the Fe_4 cluster, the interaction of O_2 leads to the dissociation of the O−O bond and the total spin moment reduces from 14 to 10 μ_B (*viz.* Figure 3b). The energy released in the reaction is 4.28 eV which is close to Fe + O_2 reaction. Another isomer, where the O−O bond does not break but elongates significantly (1.48 Å), is found to be 1.46 eV higher in energy. Thus, it is inferred that the interaction of O_2 with Fe leads to the dissociation of the O−O bond resulting in atomic adsorption of O with Fe.

In the next step we have calculated the interaction of O_2 with $(BN)_{36}$, $Fe(BN)_{36}$, and $Fe_4(BN)_{36}$ clusters. The reaction of O_2 with the $(BN)_{36}$ cluster was carried out by placing it at different locations on the cage (on top of B and N, tetragonal and hexagonal rings of the cage). In all cases it is found that the molecular O_2 does not bind on the cage, instead, goes away from its surface (A typical representative illustration is shown in Supporting Information, Figure S2). Subsequent to this verification, that the O_2 molecule does not adsorb on the empty cage $(BN)_{36}$ cluster, the reaction of O_2 with $Fe(BN)_{36}$ cluster was carried out. Unlike in the case of empty cage $(BN)_{36}$ cluster, it is found that the O_2 molecule is adsorbed on the $Fe(BN)_{36}$ cluster. The lowest energy configuration shows that (Figure 3c) the O−O bond is placed parallel to the hexagonal ring (close to the Fe atom) from outside and the O−O bond is elongated up to 1.47 Å (peroxo type[49]). The energy released in this reaction is calculated to be 2.04 eV. The next isomer, where the O_2 molecule is adsorbed in an elbow-shaped orientation is found to be 1.12 eV higher in energy. Another isomer, where the O_2 molecules adsorbs after breaking the O−O bond (shown in Figure 3c) is found to be 1.65 eV higher in energy. In this context it may be recalled that the interaction of O_2 with an uncoated Fe atom results in O−O bond dissociation with large energy release. However, when Fe is incorporated inside the $(BN)_{36}$ cage, the interaction of O_2 shows intermediate interaction energy. Unlike, the empty cage

$(BN)_{36}$ cluster, the HOMO of the $Fe(BN)_{36}$ is found to be localized on the Fe atom and the B and N atoms of the nearest Fe (shown in Supporting Information, Figure S1). Thus it may be argued that the incorporation of the Fe atom inside the $(BN)_{36}$ cluster can activate the nearest hexagon ring, which in turn favors the weak adsorption of the O_2 molecule. When similar studies were repeated for the $Fe_4(BN)_{36}$ cluster, the adsorption behavior of the O_2 molecule was found to be the same. For the $Fe_4(BN)_{36}$ cluster, the lowest energy configuration shows that the O_2 molecule binds on the $Fe_4(BN)_{36}$ cage in parallel orientation (shown in Figure 3d) by stretching the O−O bond up to 1.52 Å. The second and third higher energy isomers corresponds to the elbow-shaped and O−O bond scission with the relative stability (ΔE) of 0.65 and 0.77 eV, respectively, as shown in Figure 3. We have summarized the energetics and spin moments of the O_2 interaction with free and encapsulated Fe clusters in Table S2 of the Supporting Information.

Once it is realized that the adsorption of O_2 on the $Fe(BN)_{36}$ or $Fe_4(BN)_{36}$ clusters leads to weakening of the O−O bond strength, it is of worth to investigate the applicability of these clusters for oxidative catalysis. To verify this fact we have carried out the CO oxidation reaction which has been used widely as prototype examples.[11−13] The oxidation of the CO molecule occurs *via* either of the two following mechanisms. In most cases it proceeds *via* the so-called Langmuir−Hinshelwood (L−H) mechanism where the reacting species are coadsorbed before undergoing the reaction. This involves formation of an intermediate complex and desorption of the CO_2 molecule. In the second case which is known as Elay−Rideal (E−R) mechanism, the O_2 molecule is first adsorbed on the catalyst support and the gas phase CO molecules undergoes an oxidation *via* the detachment of the O−O bond. Irrespective of the mechanisms followed, the key steps of the CO oxidation are (i) the weakening or breaking of the O−O bond in the adsorbed O_2 molecule and (ii) the formation of the CO_2 molecule.

To investigate the reaction of CO with O_2, we have carried out the geometry optimization using both mechanisms as mentioned above. In the case of coadsorption (L−H mechanism), we have explored several possible orientations as shown in Supporting Information, Figures S3 and S4. The optimized geometries showed a complex formation between CO and O_2 without leaving CO_2 as the oxidation product. On the other hand when the O_2 molecule is first adsorbed on the $Fe(BN)_{36}$ cluster, the subsequent approach of the CO molecule leads to the oxidation to CO_2 *via* the detachment of the O−O bond (shown in Figure 4). The energy released in this process $\{Fe(BN)_{36}O_2 + CO \rightarrow Fe(BN)_{36}O + CO_2\}$ is calculated to be 2.68 eV. After this, when another CO molecule is placed on the $Fe(BN)_{36}$−O complex (B−O = 1.25 Å), the CO_2 formation does not occur spontaneously. However, the total energy calculation for the reaction of $\{Fe(BN)_{36}O + CO \rightarrow Fe(BN)_{36} + CO_2\}$ indicates that the CO_2 removal is energetically favorable as the energy released is estimated to be 1.82 eV, indicating the existence of an activation barrier in the process. We have adopted the nudge elastic band (NEB)[63,64] method to calculate this activation energy. Total four images between the reactant and product states were used to find out the minimum energy path (MEP) in this process (shown in Figure 5). Using this method the energy barrier is calculated to be 0.51 eV for the formation of a second CO_2 molecule. For the $Fe_4(BN)_{36}$ cluster, we have performed similar steps, that is, we have optimized the geometries of the two CO molecule on the $Fe_4(BN)_{36}$−O−O complex sequentially (shown in Figure 4). The results suggest that unlike in the case of the $Fe(BN)_{36}$ cluster, where the second CO_2 formation requires a small activation energy for the formation of a CO_2 molecule, in this case, both steps undergoes spontaneously. It should be mentioned here that the B−O distance in the intermediate $Fe_4(BN)_{36}$−O species is found to be 1.38 Å, which is significantly larger than what has been found for $Fe(BN)_{36}$−O complex. The weaker bond strength of the O atom with the B atom of the cage is responsible for the spontaneous removal of oxygen leading to the formation of a second CO_2 molecule.

We believe that the primary reason for such catalytic activity of the inert $(BN)_{36}$ cage is the activa-

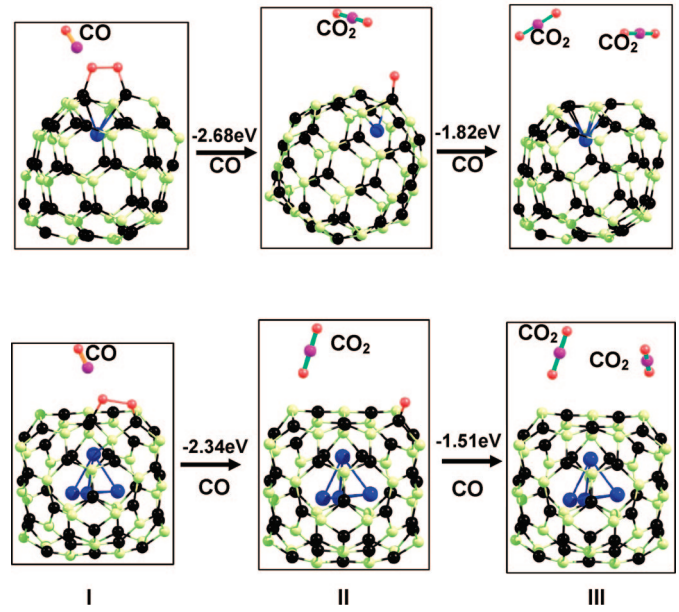

Figure 4. Step by step illustration of the CO oxidation process on the $Fe(BN)_{36}O_2$ and $Fe_4(BN)_{36}O_2$ clusters: (I) Interaction of CO with $Fe(BN)_{36}O_2$ or $Fe_4(BN)_{36}O_2$ cluster; (II) formation of first CO_2 molecule, and (III) formation of the second CO_2 molecule. It may be noted that for $Fe(BN)_{36}O_2$, the second CO_2 formation occurs *via* an activation barrier of 0.13 eV.

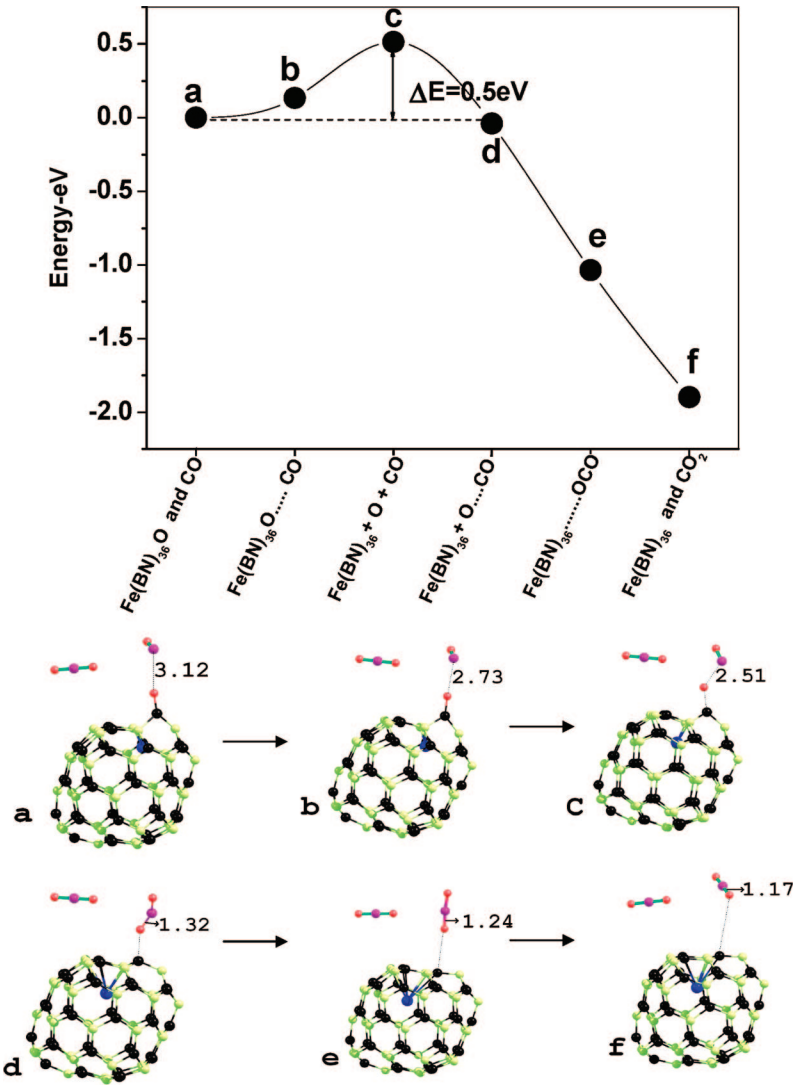

Figure 5. The reaction path of the second CO_2 molecule from the $Fe(BN)_{36}$−O intermediate complex. The nudge elastic band method (NEB) was used to calculate the MEP. The CO−O bond distances shown in the figure are given in angstroms.

tion of the nearest BN hexagonal ring by the encapsulated Fe. Once the cage atoms become active, it adsorbs the O_2 molecule resulting in weakening of the O−O bond. This underlies the catalytic activity of the $Fe(BN)_{36}$ cage toward oxidation of CO into CO_2. On the basis of these results it is predicted that if bulk iron is coated with a very thin layer (monolayer) of boron nitride then it can be used as an oxidative catalyst, but a multilayer coating will provide oxidation resistance to Fe. We believe that these theoretical predictions will encourage new experiments to design a novel catalyst based on easily available and cost-effective iron particles.

CONCLUSION

In summary, we have demonstrated a novel oxidative catalyst based on iron clusters encapsulated inside the inert boron nitride cage. The results show that the Fe_4 cluster can be stabilized inside the $(BN)_{36}$ cluster with reduction in the spin moment from 14 to 10 μ_B. The influence of the iron incorporation inside the boron nitride cage leads to the appearance of localized energy states of the iron clusters in the energy gap of the $(BN)_{36}$ cluster leading to the activation of the inert cage. This inference has been corroborated by the adsorption of O_2 molecules on the outer surface of the boron nitride cage without dissociation of the O−O bond. Further reaction of the gas phase CO molecules leads to the formation of CO_2 spontaneously. The reaction mechanism has been investigated *via* the L−H and E−R routes, and the minimum energy path calculations are performed using the elastic band method. The results reveal that the CO_2 formation takes place *via* the E−R route. Thus, the presence of Fe nanoparticles inside the BN fullerene results in the activation of the inert cage, which can be used in the oxidation catalysis.

COMPUTATIONAL DETAILS

The total energy calculation and geometry optimization were performed under density functional theory formalism and plane wave basis set as implemented in the Vienna *ab initio* simulation package (VASP).[50−52] The electron−ion interaction was described by the all-electron projector augmented wave (PAW) method,[53] as implemented in VASP by Kresse and Joubert.[54] The PAW pseudopotential was generated taking scalar relativistic corrections into account. The spin-polarized generalized gradient approximation[55] has been used to calculate the exchange-correlation energy. The cut-off energy for the plane wave basis set was fixed at 400 eV for all calculations performed in this study. A simple cubic supercell of side 15 Å was used to ensure that the periodically repeated cluster images do not interact with each other. The brillouin zone integrations are carried out at the Γ point only. The geometry of the clusters has been determined by ionic relaxation, using a conjugate gradient minimization and the exact Hellmann−Feynman forces. The geometries are considered to be converged when the force on each ion becomes 0.005 eV/ Å or less. The total energy convergence was tested with respect to the plane-wave basis set size and simulation cell size, and the total energy was found to be accurate to within 1 meV. To check the effect of relativistic corrections, total energy calculations were repeated after incorporating the spin−orbit coupling term. However, no significant changes were found on the binding energies of these clusters.

Acknowledgment. The authors thank the staff members of the supercomputing facility of the Computer Division, BARC, for their support during this work.

Supporting Information Available: Comparison of the calculated (experimental) values of the bond lengths and bond energy of O_2, CO, and CO_2 molecules; calculated interaction energy of O_2 with free and encapsulated Fe atoms/clusters; HOMO structures of $(BN)_{36}$, $Fe(BN)_{36}$, and $Fe_4(BN)_{36}$ clusters; molecule−cluster reaction intermediate structures. This material is available free of charge *via* the Internet at http://pubs.acs.org.

REFERENCES AND NOTES

1. Greeley, J.; Norskov, J. K.; Mavrikakis, M. Electronic Structure and Catalysis on Metal Surfaces. *Annu. Rev. Phys. Chem.* **2002**, *53*, 319–348.
2. Honkala, K.; Hellman, A.; Remediakis, I. N.; Logadottir, A.; Carlsson, A.; Dahl, S.; Christensen, C. H.; Norskov, J. K. Ammonia Synthesis From First-Principles Calculations. *Science* **2005**, *307*, 555–558.
3. Whitten, J. L.; Yang, H. Theory of Chemisorption and Reactions on Metal Surfaces. *Surf. Sci. Rep.* **1996**, *24*, 55–124.
4. Brown, A. W.; King, D. A. NO Chemisorption and Reactions on Metal Surfaces: A New Perspective. *J. Phys. Chem. B* **2000**, *104*, 2578–2595.
5. Vang, R. T.; Honkala, K.; Dahl, S.; Vestergaard, E. K.; Schnadt, J.; Laegsgaard, E.; Clausen, B. S.; Norskov, J. K.; Besenbacher, F. Controlling the Catalytic Bond-Breaking Selectivity of Ni Surfaces by Step Blocking. *Nat. Mater.* **2005**, *4*, 160–162.
6. Bernhardt, T. M.; Heiz, U.; Landman, U. Chemical and Catalytic Properties of Size-Selected Free and Supported Clusters. In *Nanocatalysis*; Heiz U., Landman U., Eds.; Springer: Heidelberg, 2006; pp 1−192.
7. Heiz, U.; Schneider, W. D. Physical Chemistry of Supported Clusters. In *Metal Clusters at Surfaces: Structure, Quantum Properties, Physical Chemistry*; Meiwes-Broer, K. H., Ed.; Springer-Verlag: Berlin-Heidelberg, 2000; pp 237−273..
8. Bonn, M.; Funk, S.; Hess, Ch.; Denzler, D. N.; Stampfl, C.; Scheffler, M.; Wolf, M.; Ertl, G. Phonon-Versus Electron-Mediated Desorption and Oxidation of CO on Ru(0001). *Science* **1999**, *285*, 1042–1045.
9. Over, H.; Muhler, M. Catalytic CO Oxidation Over Ruthenium - Bridging the Pressure Gap. *Prog. Surf. Sci.* **2003**, *72*, 3–17.
10. Yoon, B.; Hakkinen, H.; Landman, U.; Worz, A. S.; Antonietti, J. M.; Abbet, S.; Judai, K.; Heiz, U. Charging Effects on Bonding and Catalyzed Oxidation of CO on Au_8 Clusters on MgO. *Science* **2005**, *307*, 403–407.
11. Zhang, C.; Yoon, B.; Landman, U. Predicted Oxidation of CO Catalyzed by Au Nanoclusters on A Thin Defect-Free MgO Film Supported on a Mo(100) Surface. *J. Am. Chem. Soc.* **2007**, *129*, 2228–2229.
12. Landman, U.; Yoon, B.; Zhang, C.; Heiz, U.; Arnes, M. Factors in Gold Nanocatalysis: Oxidation of CO in the Non-Scalable Size Regime. *Top. Catal.* **2007**, *44*, 145–158.
13. Socaciu, L. D.; Hagen, J.; Bernhardt, T. M.; Woste, L.; Heiz, U.; Landman, U. Catalytic CO Oxidation by Free Au_{2-}: Experiment and Theory. *J. Am. Chem. Soc.* **2003**, *125*, 10437–10445.
14. Gorin, D. J.; Toste, F. D. Relativistic Effects in Homogeneous Gold Catalysis. *Nature* **2007**, *446*, 395–403.
15. Huber, B.; Koskinen, P.; Hakkinen, H.; Moseler, M. Oxidation of Magnesia-Supported Pd-Clusters Leads to the Ultimate Limit of Epitaxy With a Catalytic Function. *Nat. Mater.* **2006**, *5*, 44–47.
16. Valden, M.; Lai, X.; Goodman, D. W. Onset of Catalytic Activity of Gold Clusters on Titania With the Appearance of Nonmetallic Properties. *Science* **1998**, *281*, 1647–1650.
17. Oku, T.; Naritab, I.; Nishiwakic, A.; Koid, N. Atomic Structures, Electronic States and Hydrogen Storage of Boron Nitride Nanocage Clusters, Nanotubes and Nanohorns. *Diffus. Defect Data, Pt. A* **2004**, *226−228*, 113–140.
18. Oku, T.; Nishiwaki, A.; Narita, I.; Gonda, M. Formation and Structure of $B_{24}N_{24}$ Clusters. *Chem. Phys. Lett.* **2003**, *380*, 620–623.
19. Oku, T.; Narita, I.; Nishiwaki, A. Synthesis, Atomic Structures, and Electronic States of Boron Nitride Nanocage Clusters and Nanotubes. *Mater. Manuf. Process.* **2004**, *19*, 1215–1239.
20. Oku, T.; Narita, I. Calculation of H_2 Gas Storage for Boron Nitride and Carbon Nanotubes Studied from the Cluster Calculation. *Physica B* **2002**, *323*, 216–218.
21. Oku, T.; Kuno, M.; Kitahara, H.; Narita, I. Formation, Atomic Structure and Properties of Boron Nitride and Carbon Nanocage Fullerene Materials. *Int. J. Inorg. Mater.* **2001**, *3*, 597–612.
22. Narita, I.; Oku, T. Synthesis of Boron Nitride Nanotubes by Using YB_6 Powder. *Solid State Commun.* **2002**, *122*, 465–468.
23. Narita, I.; Oku, T. Effects of Catalytic Metals for Synthesis of BN Fullerene Nanomaterials. *Diamond Relat. Mater.* **2003**, *12*, 1146–1150.
24. Oku, T.; Hiraga, K.; Matsuda, T.; Hirai, T.; Hirabayashi, M. Twin Structures of Rhombohedral and Cubic Boron Nitride Prepared by Chemical Vapor Deposition Method. *Diamond Relat. Mater.* **2003**, *12*, 1138–1145.
25. Oku, T.; Hirano, T.; Kuno, M.; Kusunose, T.; Niihara, K.; Suganuma, K. Synthesis, Atomic Structures and Properties of Carbon and Boron Nitride Fullerene Materials. *Mater. Sci. Eng., B* **2000**, *74*, 206–217.
26. Oku, T.; Suganuma, K. High-Resolution Electron Microscopy and Structural Optimization of C_{36}, $B_{36}N_{36}$ and $Fe_{36}N_{36}$ Clusters. *Diamond Relat. Mater.* **2001**, *10*, 1205–1209.
27. Oku, T.; Kuno, M.; Narita, I. Molecular Dynamics Calculation of H_2 Gas Storage in C_{60} and $B_{36}N_{36}$ Clusters. *Diamond Relat. Mater.* **2002**, *11*, 945–948.
28. Oku, T.; Narita, I.; Nishiwaki, A. Formation and Structures of $B_{36}N_{36}$ and $Y@B_{36}N_{36}$ Clusters Studied by High-Resolution Electron Microscopy and Mass Spectrometry. *J. Phys. Chem. Solids* **2004**, *65*, 369–372.
29. Oku, T.; Narita, I.; Tokoro, H. Synthesis and Magnetic Property of Boron Nitride Nanocapsules Encaging Iron and Cobalt Nanoparticles. *J. Phys. Chem. Solids* **2006**, *67*, 1152–1156.
30. Han, W.; Zettl, A. Functionalized Boron Nitride Nanotubes with a Stannic Oxide Coating: A Novel Chemical Route to Full Coverage. *J. Am. Chem. Soc.* **2003**, *125*, 2062–2063.
31. Man, W.; Chang, C. W.; Zettl, A. Encapsulation of One-Dimensional Potassium Halide Crystals Within BN Nanotubes. *Nano Lett.* **2004**, *4*, 1355–1357.
32. Zhi, C.; Bando, Y.; Tang, C.; Kuwahara, H.; Golberg, D. Grafting Boron Nitride Nanotubes: From Polymers to Amorphous and Graphitic Carbon. *J. Phys. Chem. C* **2007**, *111*, 1230–1233.
33. Golberg, D.; Bando, Y.; Kurashima, K.; Sasaki, T. Boron-Doped Carbon Fullerenes and Nanotubules formed Through Electron Irradiation-Induced Solid-State Phase Transformation. *Appl. Phys. Lett.* **1998**, *72*, 2108–2110.
34. Golberg, D.; Han, W.; Bando, Y.; Bourgeois, L.; Kurashima, K.; Sato, T. Fine Structure of Boron Nitride Nanotubes Produced from Carbon Nanotubes by a Substitution Reaction. *J. Appl. Phys.* **1999**, *86*, 2364–2366.
35. Alexandre, S. S.; Mazzoni, M. S. C.; Chacham, H. Stability, Geometry, and Electronic Structure of the Boron Nitride $B_{36}N_{36}$ Fullerene. *Appl. Phys. Lett.* **1999**, *75*, 61–63.
36. Alexandre, S. S.; Nunes, R. W.; Chacham, H. Energetics of the Formation of Dimers and Solids of Boron Nitride Fullerenes. *Phys. Rev. B* **2002**, *66*, 854061–854065.
37. Wang, Q.; Sun, Q.; Oku, T.; Kawazoe, Y. First-Principles Study of La-$B_{36}N_{36}$ Cage. *Physica B* **2003**, *339*, 105–109.
38. Nigam, S.; Majumder, C. Magnetic Needles Encapsulated Inside $(BN)_{36}$ Cage: Prediction of Atomic, Electronic, and Magnetic Structure from First Principle Calculations. *Appl. Phys. Lett.* **2007**, *91*, 2231121–2231123.
39. Stephan, O.; Bando, Y.; Loiseau, A.; Willaime, F.; Shramchenko, N.; Tamiya, T.; Sato, T. Formation of Small Single-Layer and Nested BN Cages Under Electron Irradiation of Nanotubes and Bulk Material. *Appl. Phys. A: Mater. Sci. Process.* **1998**, *67*, 107–111.

40. Terauchi, M.; Tanaka, M.; Matsada, H.; Takeda, M.; Kimura, K. Helical Nanotubes of Hexagonal Boron Nitride. *J. Electron Microsc.* **1997**, *46*, 75–78.
41. Bando, Y.; Ogawa, K.; Golberg, D. Insulating 'Nanocables': Invar Fe-Ni Alloy Nanorods Inside BN Nanotubes. *Chem. Phys. Lett.* **2001**, *347*, 349–354.
42. Tang, C.; Bando, Y.; Golberg, D.; Ding, X.; Qi, S. Boron Nitride Nanotubes Filled With Ni and $NiSi_2$ Nanowires *in Situ*. *J. Phys. Chem. B* **2003**, *107*, 6539–6543.
43. Xu, F.; Bando, Y.; Golberg, D.; Hasegawa, M.; Mitome, M. Phases and Crystallization of Encapsulated Cobalt Nanorods Inside BN Nanotubes. *Acta Mater.* **2004**, *52*, 601–606.
44. Peng, G. W.; Huan, A. C. H.; Feng, Y. P. Energetic and Magnetic Properties of Transition-Metal Nanowire Encapsulated $B_xC_yN_z$ Composite Nanotubes. *Appl. Phys. Lett.* **2006**, *88*, 1931171–1931173.
45. Batista, R. J. C.; Mazzoni, M. S. C.; Chacham, H. Boron Nitride Fullerene $B_{36}N_{36}$ Doped With Transition Metal Atoms: First-Principles Calculations. *Phys. Rev. B* **2007**, *75*, 354171–354175.
46. Koia, N.; Oku, T.; Nishijimab, M. Fe Nanowire Encapsulated in Boron Nitride Nanotubes. *Solid State Commun.* **2005**, *136*, 342–345.
47. Nakao, K.; Watanabe, O.; Sasaki, T.; Ito, S.; Tomishige, K.; Kunimori, K. CO Oxidation on Pd(111), Pt(111), and Rh(111) Surfaces Studied by Infrared Chemiluminescence Spectroscopy. *Surf. Sci.* **2007**, *601*, 3796–3800.
48. Feibelman, P. J.; Hammer, B.; Norskov, J. K.; Wagner, F.; Scheffler, M.; Stumpf, R.; Watwe, R.; Dumesic, J. The Co/Pt(111) Puzzle. *J. Phys. Chem. B* **2001**, *105*, 4018–4025.
49. Gutsev, G. L.; Rao, B. K.; Jena, P. Systematic Study of Oxo, Peroxo, and Superoxo Isomers of 3d-Metal Dioxides and Their Anions. *J. Phys. Chem. A* **2000**, *104*, 11961–11971.
50. Kresse, G.; Furthmuller, J. Efficient Iterative Schemes for *ab-Initio* Total-Energy Calculations Using a Plane-Wave Basis Set. *Phys. Rev. B* **1996**, *54*, 11169–11186.
51. Kresse, G.; Furthmuller, J. Efficiency of Ab-Initio Total Energy Calculations For Metals and Semiconductors Using A Plane-Wave Basis Set. *Comput. Mater. Sci.* **1996**, *6*, 15–50.
52. Vanderbilt, D. Soft Self-Consistent Pseudopotential in A Generalised Eigenvalue Formalism. *Phys. Rev. B* **1990**, *41*, 7892–7895.
53. Blochl, P. E. Projector Augmented-Wave Method. *Phys. Rev. B* **1994**, *50*, 17953.
54. Kresse, G.; Joubert, D. From Ultrasoft Pseudopotentials to the Projector Augmented-Wave Method. *Phys. Rev. B* **1999**, *59*, 1758–1775.
55. Perdew, J. P.; Burke, K.; Ernzerhof, M. Generalized Gradient Approximation Made Simple. *Phys. Rev. Lett.* **1996**, *77*, 3865–3868.
56. Lan, Y.-Z.; Cheng, W. D.; Wu, D. S.; Li, X. D.; Zhang, H.; Gong, Y. J.; Shen, J.; Li, F. F. Theoretical Studies of Third-Order Nonlinear Optical Response for $B_{12}N_{12}$, $B_{24}N_{24}$ And $B_{36}N_{36}$ Clusters. *J. Mole. Struct.: Theochem.* **2005**, *730*, 9–15.
57. Koi, N.; Oku, T. Molecular Orbital Calculations of Hydrogen Storage in Carbon and Boron Nitride Clusters. *Sci. Technol. Adv. Mater.* **2004**, *5*, 625–628.
58. Koi, N.; Oku, T. Hydrogen Storage in Boron Nitride and Carbon Clusters Studied by Molecular Orbital Calculations. *Solid State Commun.* **2004**, *131*, 121–124.
59. Zope, R. R.; Baruah, T.; Pederson, M. R.; Dunlap, B. I. Theoretical Infrared, Raman, and Optical Spectra of The $B_{36}N_{36}$ Cage. *Phys. Rev. A* **2005**, *71*, 252011–252014.
60. Zope, R. R.; Dunlap, B. I. Are Hemispherical Caps of Boron-Nitride Nanotubes Possible. *Chem. Phys. Lett.* **2004**, *386*, 403–407.
61. Sun, Q.; Wang, Q.; Jena, P. Storage of Molecular Hydrogen in B-N Cage: Energetics and Thermal Stability. *Nano Lett.* **2005**, *5*, 1273–1277.
62. Hobbs, D.; Kresse, G.; Hafner, J. Fully Unconstrained Noncollinear Magnetism Within The Projector Augmented-Wave Method. *Phys. Rev. B* **2000**, *62*, 11556–11570.
63. Mills, G.; Jonsson, H.; Schenter, G. K. Reversible Work Transition State Theory: Application to Dissociative Adsorption of Hydrogen. *Surf. Sci.* **1995**, *324*, 305–337.
64. Jonsson, H.; Mills, G.; Jacobsen, K. W. Nudged Elastic Band Method For Finding Minimum Energy Paths of Transitions. In *Classical And Quantum Dynamics In Condensed Phase Simulations;* Berne, B. J., Ciccotti, G., Coker, D. F., Eds.; World Scientific: Rivers Edge, NJ, 1998; pp 385−404.